ISSN 0027-1349, Moscow University Physics Bulletin, 2018, Vol. 73, No. 1, pp. 75–82. © Allerton Press, Inc., 2018.
Original Russian Text © V.P. Zarubin, A.S. Bychkov, A.A. Karabutov, V.A. Simonova, I.A. Kudinov, E.B. Cherepetskaya, 2018, published in Vestnik Moskovskogo Universiteta, Seriya 3: Fizika, Astronomiya, 2018, No. 1, pp. 76–83.

Real-Time Laser Ultrasound Tomography for Profilometry of Solids

V. P. Zarubin[a, b, *], A. S. Bychkov[a, b], A. A. Karabutov[a, b], V. A. Simonova[a, c, **], I. A. Kudinov[a], and E. B. Cherepetskaya[a]

[a] *International Laser Center, Moscow State University, Moscow, 119991 Russia*
[b] *National Research Technological University MISiS , Moscow, 119049 Russia*
[c] *Institute on Laser and Information Technologies, Russian Academy of Sciences, Shatura, Moscow oblast, 140700 Russia*
**e-mail: zarubin.vasily@gmail.com,*
***e-mail: vas@optoacoustics.ru*

Received December 20, 2016; in final form, March 31, 2017

Abstract—We studied the possibility of applying laser ultrasound tomography for profilometry of solids. The proposed approach provides high spatial resolution and efficiency, as well as profilometry of contaminated objects or objects submerged in liquids. The algorithms for the construction of tomograms and recognition of the profiles of studied objects using the parallel programming technology NDIVIA CUDA are proposed. A prototype of the real-time laser ultrasound profilometer was used to obtain the profiles of solid surfaces of revolution. The proposed method allows the real-time determination of the surface position for cylindrical objects with an approximation accuracy of up to 16 μm.

Keywords: profilometry, laser ultrasound, laser ultrasound tomography.
DOI: 10.3103/S0027134918010150

INTRODUCTION

The problem of surface profile inspection is especially important in the production of objects with complex shapes. Profilometry can be performed using various methods, which can be separated into two groups: contact and noncontact methods.

Initially, mechanical profilometers were the most widespread, due to their high measurement precision, reliability, and the relative simplicity of their use [1, 2]. Low inspection performance and difficulties in processing rough and "soft" objects require other profilometry methods.

This problem can be solved using optical and ultrasonic methods of noncontact profilometry. The most widespread methods of noncontact profilometry are, first of all, laser interferometry and laser triangulation. The advantages of optical profilometers are the spatial resolution to fractions of nanometers in combination with a relatively high scanning rate [3–5]. An even higher inspection performance is achieved using digital processing of optical images.

The application of optical profilometry requires the preparation (washing) of the object surface, which, generally speaking, may substantially increase the cost of profilometry. The real-time sample profile inspection implies the study of contaminated samples, including those that are submerged into nontransparent liquids (for example, lubricants and coolants). The application of optical profilometry in this case is inefficient. It is reasonable to apply ultrasound profilometry.

The most widespread method of ultrasound profilometry is acoustic microscopy [6]. This method is applied for inspecting elements of microelectronics and objects submerged in liquids (as a rule, distilled water); it provides sufficiently high (up to submicron) spatial resolution. The application of ultrasound microscopy for shape inspecting in mechanical production is not as efficient because of a rather strong attenuation of high-frequency (100 MHz and higher) ultrasound in organic liquids, and, as a consequence, reduction of the profilometry resolution; the typical value is ~10 μm. This, however, is quite sufficient for a wide range of inspected components.

In this study, we use laser ultrasound tomography for profilometry of solids submerged in liquids. The method of laser ultrasound tomography applied for profilometry is called laser ultrasound profilometry. Laser ultrasound profilometry has a number of advantages compared to traditional ultrasound visualization of sample profiles.

Laser ultrasound diagnostics assumes generation of the probing ultrasonic pulse due to absorption of the laser pulse in the surface layer of the studied medium

(or a special optical acoustic generator) and registration of the transmitted or scattered ultrasonic signal with high temporal resolution. The time profile and amplitude of the probing ultrasonic pulse depend on the light absorption coefficient in the optical acoustic generator, the time profile of the laser pulse, and the absorbed laser energy density.

The advantage of the laser ultrasound method is the possibility of the generation of short high-power aperiodic ultrasonic pulses, which is impossible with common ultrasound generators [7]. The short duration of the probing pulse results in the higher longitudinal spatial resolution, preserving a reasonable signal bandwidth. One of the disadvantages of the traditional ultrasound diagnostic methods is the "dead zone" in which the signal reflected from an inhomogeneity is superposed with the probing signal. The aperiodic character of the probing pulse provides substantial reduction of the size of the "dead zone". Moreover, in laser ultrasound diagnostics, ultrasonic transducers operate in the reception mode only, which provides high temporal resolution.

The advantages of the laser ultrasound approach in profilometry, compared to traditional ultrasound methods are as follows:

(i) increased spatial resolution, compared to the contact and optical methods;

(ii) profilometry of contaminated and submerged objects.

The proposed method is a development of laser ultrasound profilometry with a single piezo element [8].

The application of the tomographic approach increases the performance compared to a single piezo element; the profile of an extended surface area is taken at one time. Obviously, the complexity of signal processing for tomograms also increases noticeably.

1. METHOD

In this study, we developed a prototype of a laser ultrasound profilometer capable of operating on a production line. This requires the development of the principles of laser ultrasound profilometry, as well as algorithms for construction and processing of laser ultrasound images and sample profiles.

In [8], the time-of-flight laser ultrasound method, in which the reflected signal was recorded using a single piezo element, was applied for profilometry of solids. In essence, laser ultrasound profilometry is a development of the time-of-flight laser ultrasound profilometry via a larger number of receiving elements, as was performed earlier for laser ultrasound tomography of biological objects [9, 11]. The basic principle of the method is irradiation of the object by a thermoacoustically generated ultrasonic beam, registration of scattered and reflected waves by the antennas of detectors, and computer reconstruction of the object image from the tomogram using specialized algorithms.

The schematic diagram of the experimental apparatus, which is a prototype of a laser ultrasound profilometer, is shown in Fig. 1. The system consists of *1* a *Q*-switched Nd:YAG laser (Quantel, United States) with $\lambda = 1064$ nm, a pulse repetition rate of 20 Hz, and an energy per pulse of 10 mJ; *2* a laser radiation transmission system with an optical fiber; *3* a combined power supply unit for an antenna and electric signal amplifier; *4* a high speed multichannel data acquisition and processing system based on NI FlexRIO architecture, which contains precision ADC (with a discretization rate of 50 MHz) and provides conversion of electric signals from piezoelectric receiving elements into the digital form, their storage, averaging, and transmission via a high speed communication line to a PC; *5* a data-processing system including a PC connected via a high-speed data transmission line with the data acquisition and processing system, the CUDA (Computer Unified Device Architecture) software–hardware platform, and the corresponding software for digital data reception, processing, and image construction, as well as interactive control of the data transmission and processing; *6* a receiving antenna containing the optoacoustic converter (optoacoustic generator) and the grid of broadband piezoelectric receiving elements; *7* a system of automated three-dimensional positioning of the receiving antenna and the studied object. The system provides variation of the relative position of the object in the holder with a precision of up to 0.01 mm.

A data-acquisition and processing system *4* and three-dimensional positioning system *7* are controlled from PC *5*.

The experimental multichannel system proposed in this study operates in two modes: the laser ultrasound and the optical acoustic modes [9]. For the formulated problem, however, only laser ultrasound mode is applied. In this mode laser radiation is absorbed in the material of the optoacoustic generator. Nonstationary expansion of the generator material takes place as a result of radiation absorption, which results in generation of broadband ultrasonic pulses. Ultrasonic pulses are focused by the acoustic lens on the object surface. An important condition of the installation operation is acoustic matching of all elements of the antenna acoustic path. The ultrasonic beam scattered on the inhomogeneities of the immersion liquid and the surface of the studied object, is focused by the acoustic lens on the surface of the piezoelectric receiving antenna and is recorded by the receiving elements. The piezoelectric receiving elements of the antenna are manufactured from PVDF, providing a spectral reception band of 1.6–9 MHz. This reception band provides the resolution over the depth $\Delta z = 0.1$ mm. The focal distance of the multielement antenna is $f = 40$ mm.

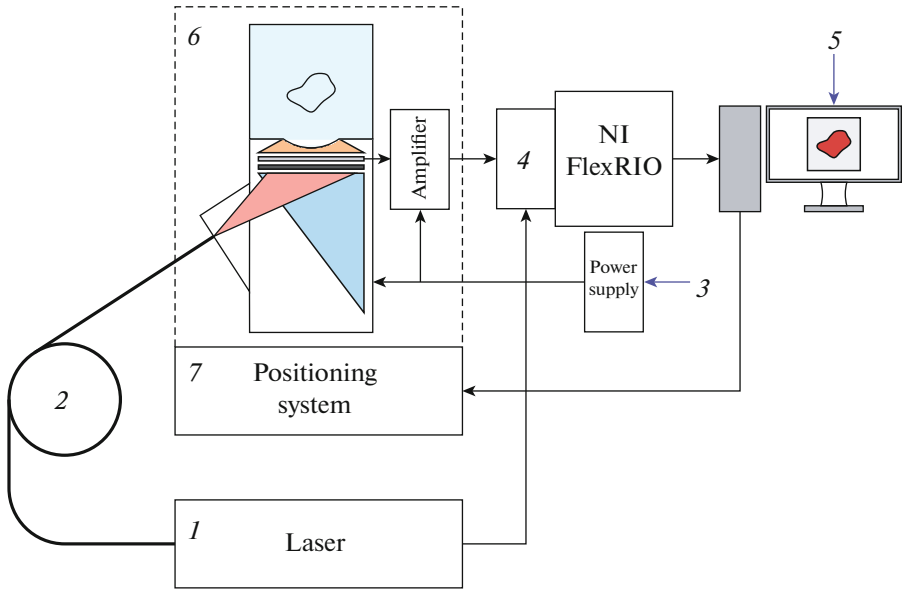

Fig. 1. A schematic diagram of the multichannel system for laser ultrasound and optoacoustic tomography (*1* laser, *2* laser radiation transmission system, *3* power supply unit, *4* data accumulation and processing system, *5* PC, *6* receiving antenna, *7* three-dimensional positioning system).

The basic methods applied for reconstruction of optoacoustic images include the model, spectral, and temporal algorithms [12]. The development of algorithms for reconstruction of laser ultrasound images encounters considerable difficulties. In this study, we applied the back-projections algorithm, heuristically modified for the laser ultrasound mode [10]. The advantage of the back-projections algorithm is the possibility of handling a small number of receiving elements, the universal character of the algorithm for different geometries of receiving elements, and the relative simplicity of the algorithm parallelization. A planar acoustic beam is used in the laser ultrasound mode. In the approximation of the planar beam its propagation can be assumed to be rectilinear; this beam is scattered at each point by point scatterers. Therefore, the back-projections formula can be written in the form

$$p_0^b(\mathbf{r}) = \sum_{i=1}^{N} \Delta\Omega_i \times b\left(\mathbf{d}_i, t = \frac{-b + z + |\mathbf{d}_i - \mathbf{r}|}{c}\right) \Big/ \sum_{i=1}^{N} \Delta\Omega_i,$$

where $p_0^b(\mathbf{r})$ is the calculated acoustic pressure at the point with the radius vector $\mathbf{r}$, $\mathbf{d}_i$ is the radius vector of the center of the receiving element, z is the longitudinal coordinate of the pixel, b is the longitudinal coordinate of the point of laser ultrasound generation, N is the number of elements, $\Delta\Omega_i$ is the solid angle at which the receiving element can be seen from the calculated point, t is the total time of acoustic-wave propagation from the generator to the calculated point and back to the piezoelectric antenna, and c is the speed of sound in water which is taken constant. It is assumed that the zero of the longitudinal coordinate corresponds to the position of the receiving antenna. The value of the back-projections $b(\mathbf{r}, t)$ can be calculated using the formula

$$b(\mathbf{d}_i, t) = -2\frac{\partial p(\mathbf{d}_i, t)}{\partial t},$$

where $p(\mathbf{d}_i, t)$ is the pressure amplitude recorded by the receiving element with the number i at the time instant t.

The result of the algorithm operation is the tomogram, a two-dimensional array containing up to 10^6 points for mapping the experimental apparatus, which shows the distribution of reflecting and scattering surfaces. Due to the high computing complexity of the tomogram, the back-projections algorithm was created using the NVIDIA CUDA parallel programming technology [13]. This approach to the algorithm provides real-time tomogram calculation. The implemented algorithm can operate in the optical acoustic and laser ultrasound modes with arc and linear antennas. Signal pre-filtering and tomogram post-processing are performed as described below.

After the laser ultrasound tomogram of the object is calculated it is necessary to construct the surface profile of the object from the tomogram. The probing pulse reflected from the object surface has the largest amplitude due to the strong acoustic mismatch of the immersion liquid (water) and the material of the studied object. Therefore, the surface profile can be constructed using the maximum of the object tomogram.

For improving the profile quality and subsequent solution of the problem of defectoscopy of solids, it is necessary to recognize and separate typical parts of the

object surface on the laser ultrasound tomogram. This image processing can be performed using computer-vision methods. In this study, the Hough transform is applied for recognition of reference rectilinear profile segments; this transform is close to the Radon transform [14]. The choice of linear segments as reference ones is determined by the simplicity of their processing, as well as the fact that linear forms are widespread in industry.

The proposed algorithm for construction and recognition of the object profile from the laser ultrasound tomogram consists of the following steps.

(1) At the first step, the maximum of pixel intensity is determined in each column of the tomogram. Note that, according to the Kotelnikov theorem, for an ADC digitization frequency of 50 MHz that is two times larger than the maximum signal frequency (in this case, 25 MHz), the maximum signal position can be determined with any accuracy. It follows from the above that local approximation of the column pixel values can be performed in the neighborhood of the found maximum; thus, the maximum can be found with higher accuracy. The set of thus-obtained maxima for each column of the laser ultrasound tomogram is called the maxima line of the tomogram.

(2) The Hough transform is used for recognition of reference straight lines on the maxima line. This transform finds rectilinear segments in the images when these segments are fragmented for some reason. The parametric equation of a straight line can be written as

$$X\cos\Theta + Y\sin\Theta = \rho,$$

where (X, Y) are the coordinates of the point in the image, and Θ and ρ are the polar angle and the distance to the line in the image with respect to some chosen point (usually, one of the corners of the image is chosen). This representation can be used to map the set of straight lines going through the points (X, Y) as the set of points in the (ρ, Θ) space. The general idea is that the transformation defines the intensity $A(\rho, \Theta)$ for each point in the (ρ, Θ) space proportional to the number of nonzero pixels on the given straight line. The function $A(\rho, \Theta)$ is called the accumulator function. The Hough transform is integrating, which results in noise averaging over the image, thus yielding a better approximation. Another advantage of the Hough transform is the possibility of development of the algorithm for the search for objects whose contours are not defined analytically, as well as the possibility of efficient parallel implementation of the algorithm using graphics processors [15]. Thus, the result of application of the transform to the image is the discrete accumulator function $A(\rho, \Theta)$, calculated with the given step. The values of this function show how high the probability of finding a straight line with the given polar angle and distance (ρ_i, Ω_i) is in the image. It follows from the above that it is possible to determine the number of straight lines and their approximate position in the profile by finding local maxima of the accumulator function.

(3) The last step of the proposed algorithm is the application of the least-squares method for finding the coefficients of the straight-line equations of the form $z_i(x) = k_i x + b_i$ (here, i is the number of the approximating straight line, x is the transverse coordinate, and z is the longitudinal coordinate, in mm), as well as the approximation errors, based on the results obtained at the previous steps. Below, we give the coefficients for the studied objects calculated from the experimental data.

Bodies of revolution, a cylinder, and a grooved cylinder from duraluminum (D16T) with the acoustic impedance $Z = 18\ 000$ kg/m^{2}s were studied as the model objects. The cylinder diameter was 14 mm, the length was 38 mm, and the groove depth and step were 2 mm. The studied object was attached along the axis, submerged into water, and moved to the focal plane of the antenna using the positioning system; the acoustic signals were then generated and recorded, the tomogram was reconstructed from these signals, and the object profile was determined.

2. DISCUSSION OF RESULTS

Figure 2 shows the comparison of the times for the sequential algorithm of tomogram construction for an AMD-A8 processor and the parallel algorithm for a NVIDIA GeForce GTX 770 video card. The construction of a tomogram with a size of 800 × 800 pixels requires approximately 25 ms, which is sufficient for real-time tomography with a large number of pixels. The algorithms were tested using the signal numerically simulated via the Rayleigh integral for the laser ultrasound scatterer.

Figure 3a shows the tomogram of the cylindrical object. The multielement receiving antenna is in the lower part of the figure. The region of positive values of the tomogram is marked in yellow, the region of values close to zero, in light green, and the region of negative values, in blue. The algorithm for construction and recognition of the surface profile proposed above was applied to the tomogram. Figure 3c shows the accumulator matrix (discrete accumulator function) on which two central symmetric maxima (the accumulator function is a function of two variables ρ and Ω represented in the form of an intensity map whose maxima correspond to the darkest pixels) corresponding to one straight line in the object tomogram are localized. The coefficients for the above equation of the straight line approximating the cylinder cross section profile (Fig. 3b) were obtained,

$$k_0 = (-1.86 \pm 0.08)\times 10^{-3},$$
$$b_0 = (-1.906 \pm 0.005)\ \text{mm}.$$

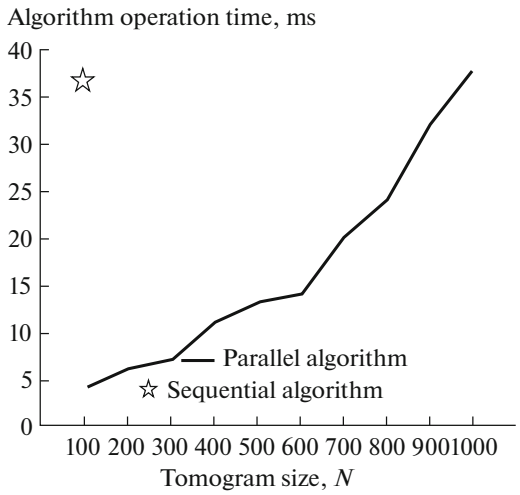

Fig. 2. The operation time of the parallel algorithm for construction of the $N \times N$ pixel tomogram. The reference point, the operation time of the sequential algorithm for the AMD-A8 processor, is marked by an asterisk.

This equation for the straight line can be used to determine by object inclination with respect to the axis of the receiving antenna. Figure 3d shows the approximation error histogram. According to these results, the accuracy of the surface approximation was 16 μm with a reliability of 95 %.

Cylinders with regular and irregular grooves were used as the model objects with a rough surface. The regular grooves on the cylinder have a step of 2 mm and a thread depth of 2 mm. The outer surface of the cylinder with regular grooves is observed in the tomogram more clearly than the inner surface. This effect is caused, first of all, by multiple reflections of the ultrasonic beam from the groove walls, which impacts the spatial resolution. The accumulator matrix of the cylinder tomogram with regular grooves contains four localized maxima (Fig. 4e) corresponding to the two longest straight lines, the inner and the outer cylinder surfaces (Fig. 4c). The following coefficients of the surface equations and the error-distribution histograms were obtained from the profile approximation by straight lines (Figs. 4g and 4i):

Outer surface: $k_1 = (-2.42 \pm 0.27) \times 10^{-3}$, $b_1 = (-2.308 \pm 0.002)$ mm.

Inner surface: $k_2 = (-1.48 \pm 0.32) \times 10^{-3}$, $b_2 = (-0.323 \pm 0.003)$ mm.

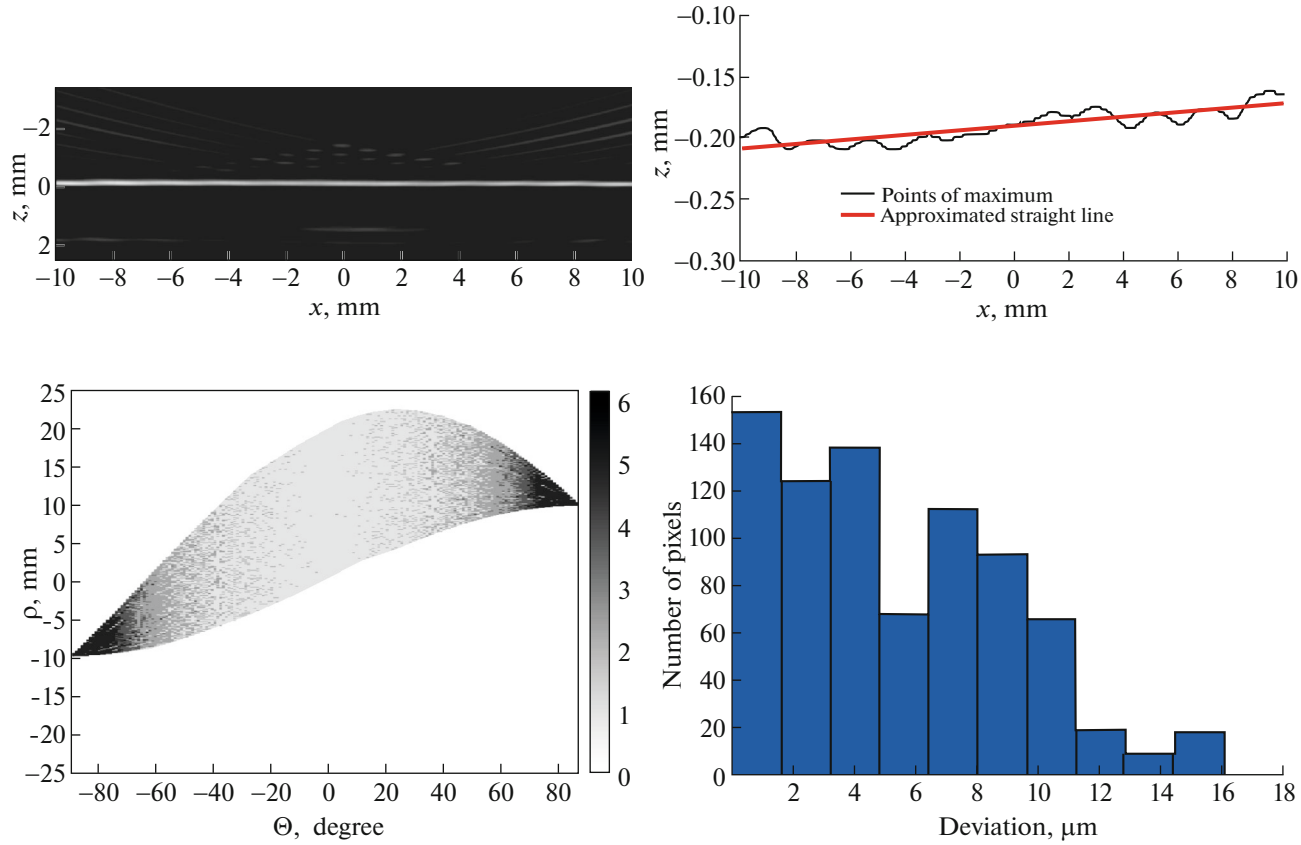

Fig. 3. The results of laser ultrasound profilometry of the cylindrical sample: (a) laser ultrasound tomogram; (b) maxima lines and approximated straight line; (c) accumulator matrix of the Hough transform (the pixel intensity is given in the logarithmic scale for clarity); (d) straight line approximation error distribution.

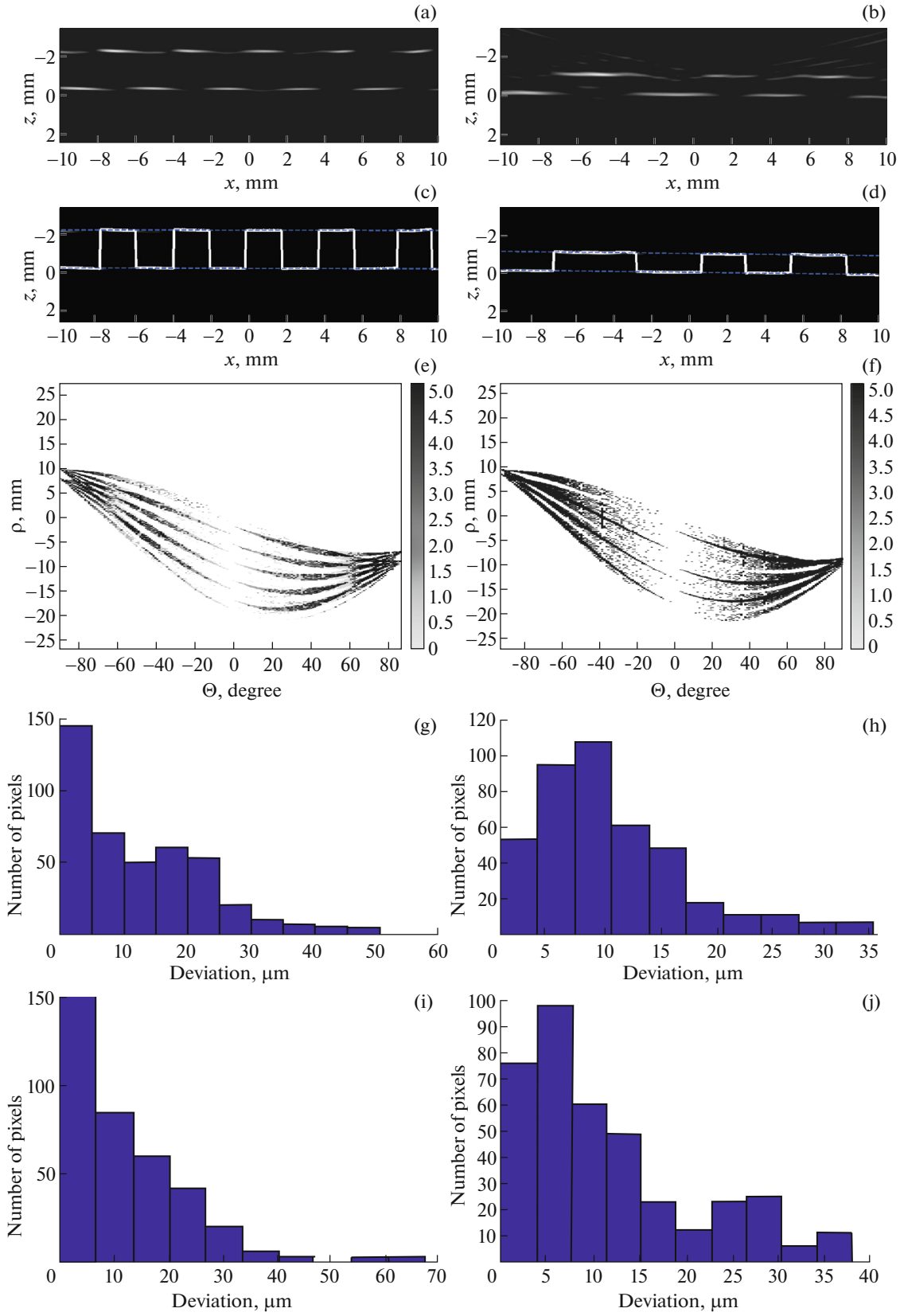

Fig. 4. The results of laser ultrasound profilometry of grooved cylindrical samples. The column on the left shows regular grooves, the column on the right shows irregular grooves. (a), (b) laser ultrasound tomograms; (c), (d) tomograms and approximating profiles; (e), (f) accumulator matrices of the Hough transform; (g), (h) longitudinal error distribution for the approximating profile of the outer cylinder surface; (i), (j) longitudinal error distribution for the approximating profile of the inner surface.

The groove depth can be determined from the equations of straight lines; it is equal to (1.985 ± 0.005) mm, which corresponds to a groove depth of 2 mm within the precision of the manufacturing of the model object. The root-mean-square approximation error for vertical lines of the regular profile (Fig. 4) is 0.21 mm; it is high because of the low transverse resolution of the multielement antenna. The low transverse resolution of the antenna is connected with the averaging of ultrasound signals over the width of each receiving element, which is equal to 1 mm.

The next studied object is the cylinder with irregular grooves. The irregular grooves have different widths from 2 mm to 7 mm and the same depth, which is equal to 1 mm. The results of the study of this cylinder (Figs. 4b, 4d, 4f, 4h, and 4j) are close to the results obtained from the cylinder with regular grooves. The main difference is that the longitudinal approximation error is reduced because of the smaller groove depth. The error of transverse approximation increases for the irregular grooves: 0.26 mm. The following coefficients of the straight-line equations that approximate the outer and inner cylinder surfaces were obtained:

Outer surface: $k_1 = (0.011 \pm 0.003)$, $b_1 = (-1.092 \pm 0.002)$ mm.

Inner surface: $k_2 = (0.011 \pm 0.001)$, $b_2 = (-1.104 \pm 0.002)$ mm.

The groove depth can be determined from these equations, it is equal to (0.988 ± 0.002) mm.

The profilometry for which the laser ultrasound method is promising requires a micron-level resolution, which results in the existence of a large number of critical factors that influence the development of the prototype of the laser ultrasound profilometer. The main problems in this field are [16, 17]:

(i) antenna configuration;

(ii) the characteristics of receiving elements and their number;

(iii) antenna calibration;

(iv) the precision of manufacturing the element and profilometer design;

(v) the local curvature and roughness of the surface;

(vi) the constant temperature and immersion liquid composition;

(vii) improved algorithms for image construction and processing.

The real-time high accuracy solution of the problem of laser ultrasound profilometry is an important step toward the development of tomographic defectoscopy of solids. These facts, which influence the profilometer resolution, determine the field of further studies aimed at the optimization of the prototype parameters, as well as the improvement of the processing algorithms.

CONCLUSIONS

In this study, we proposed a method of laser ultrasound tomography for profilometry. The algorithms for signal processing, construction of object tomograms and surface profiles, as well as the algorithm for automatic calculation of the position of curves approximating the surface cross section profile, were created. The implementation of the algorithms via the NVIDIA CUDA parallel programming technology provided real-time tomographic diagnostics with a large number of pixels on the tomogram.

A prototype of the real-time automated laser ultrasound profilometer was tested. The prototype provided determination of the surface position for cylindrical objects with an approximation accuracy of up to 16 μm and a reliability of 95%.

ACKNOWLEDGMENTS

This work was supported by NUST MISIS Competitiveness Program by the Ministry of Education and Science of the Russian Federation (K2-2017-003) and by the Russian Science Foundation (16-17-10181).

REFERENCES

1. J. M. Alves, M. C. Brito, J. M. Serra, and A. M. Vallera, Rev. Sci. Instrum. **75**, 5362 (2004). doi 10.1063/1.1821627
2. D. H. Lee and N. G. Cho, Meas. Sci. Technol. **23**, 105601 (2012). doi 10.1088/0957-0233/23/10/105601
3. T. Endo, Y. Yasuno, S. Makita, M. Itoh, and T. Yatagai, Opt. Express **13**, 695 (2005). doi 10.1364/OPEX.13.000695
4. J. Schmit, J. Reed, E. Novak, and J. K. Gimzewski, J. Opt. A: Pure Appl. Opt. **10**, 064001 (2008). doi 10.1088/1464-4258/10/6/064001
5. M. L. Dufour, G. Lamouche, V. Detalle, B. Gauthier, et al., Insight **47**, 216 (2005). doi 10.1784/insi.47.4.216.63149
6. D. Fei, D. K. Hsu, and M. Warchol, J. Nondestr. Eval. **20**, 95 (2001). doi 10.1023/A:1013550921673
7. V. E. Gusev and A. A. Karabutov, *Laser Optoacoutics* (Nauka, Moscow, 1991).
8. A. A. Karabutov, A. P. Kubyshkin, V. Ya. Panchenko, and N. B. Podymova, Proc. SPIE **3091**, 110 (1997). doi 10.1117/12.271782
9. V. A. Simonova, E. V. Savateeva, and A. A. Karabutov, Moscow Univ. Phys. Bull. **64**, 394 (2009).
10. G. Wurzinger, R. Nuster, N. Schmitner, S. Gratt, et al., Biomed. Opt. Express **4**, 1380 (2013). doi 10.1364/BOE.4.001380
11. J. Jose, R. G. H. Willemink, St. Resink, D. Piras, et al., Opt. Express **19**, 2093 (2011).

12. A. Rosenthal, V. Ntziachristos, and D. Razansky, Curr. Med. Imaging Rev. **9**, 318 (2013). doi 10.2174/15734056113096660006

13. NVIDIA CUDA programming guide. http://docs.nvidia.com/cuda/cuda-c-programming-guide/index.html.

14. R. Szeliski, *Computer Vision: Algorithms and Applications* (Springer, London, 2010). doi doi 10.1007/978-1-84882-935-0

15. G.-J. van den Braak, C. Nugteren, B. Mesman, and H. Corporaal, in *Proc. 13th Int. Conf. on Advanced Concepts for Intelligent Vision Systems, Ghent, Belgium, 2011* (Springer, 2011), p. 611. doi 10.1007/978-3-642-23687-7_5510.1007/978-3-642-23687-7_55

16. I. M. Pelivanov, V. A. Simonova, T. D. Khohlova, and A. A. Karabutov, in Proc. SPIE **7564**, 756428 (2010). doi 10.1117/12.847004

17. G. Paltauf, R. Nuster, M. Haltmeier, and P. Burgholzer, Inverse Probl. **23**, S81 (2007). doi 10.1088/0266-5611/23/6/S07

Translated by E. Baldina